
Improving Performance in Neural Networks by Dendrite-Activated Connection

Carlo Metta¹ Marco Fantozzi Andrea Papini² Gianluca Amato³ Matteo Bergamaschi⁴ Silvia Giulia Galfrè⁵
Alessandro Marchetti³ Michelangelo Vegliò³ Maurizio Parton³ Francesco Morandin⁶

Abstract

Computational units in artificial neural networks compute a linear combination of their inputs, and then apply a nonlinear filter, often a ReLU shifted by some bias, and if the inputs come themselves from other units, they were already filtered with their own biases. In a layer, multiple units share the same inputs, and each input was filtered with a unique bias, resulting in output values being based on *shared* input biases rather than individual optimal ones. To mitigate this issue, we introduce DAC, a new computational unit based on preactivation and multiple biases, where input signals undergo independent nonlinear filtering before the linear combination. We provide a Keras implementation and report its computational efficiency. We test DAC convolutions in ResNet architectures on CIFAR-10, CIFAR-100, Imagenette, and Imgewoof, and achieve performance improvements of up to 1.73%. We exhibit examples where DAC is more efficient than its standard counterpart as a function approximator, and we prove a universal representation theorem.

1. Introduction

Historically the structure of the perceptron, the artificial neural network’s fundamental computational unit, has rarely been questioned. The biological inspiration is straightforward: input signals from the dendrites are accumulated at the soma (with a linear combination), and if the result is above the activation threshold (that is, the opposite of some bias) there is a nonlinear reaction, as the neuron fires along the axon (with the activation function).

¹ISTI-CNR Pisa, Italy ²Scuola Normale Superiore, Pisa, Italy
³University of Chieti-Pescara, Italy ⁴University of Padova, Italy
⁵University of Pisa, Italy ⁶University of Parma, Italy.

Alessandro Marchetti is a PhD student enrolled in the National PhD in Artificial Intelligence, XXXVII cycle, course on Health and life sciences, organized by Campus Bio Medico University of Rome.

Contact authors at curiosailab@gmail.com.

Code at <https://github.com/curiosai/dac-dev>.

In time the early sigmoid activation function was replaced by ReLU and variants, and the biological analogy became less stringent, shifting focus on the desirable mathematical properties of the class of functions computed by the networks, like representation power and non-vanishing gradients.

This has brought us to the current situation in which most units output their signal through a nonlinear activation function which effectively destroys some information. In fact, ReLU is not invertible, as it collapses to zero all negative values. Though some of its variants may be formally invertible (leaky ReLU (Maas et al., 2013) and ELU (Clevert et al., 2016) for example), the fact that they overall perform in a way very similar to ReLU, suggests that their way of compressing negative values via a small derivative bijection leads to the same general properties of the latter.

In this paper, we propose and test a radical rethinking of the standard computational unit, where the output brings its full, uncorrupted information to the next units, and only at this point is the activation function applied, with biases specialized for each unit. From the biological point of view, this is like having the activation at the dendrites instead of at the base of the axon, and correspondingly we call the new unit ‘DAC’, for ‘Dendrite-Activated Connection’.

This kind of reversed view has already proved fruitful in the evolution from ResNets v1 (He et al., 2016a) to v2 (He et al., 2016b) when a comprehensive ablation study showed that for residual networks it is better to keep the information backbone free of activations for maximum information propagation, and preactivate the convolutional layers in the residual branch. Much earlier in the past, the celebrated LSTM (Hochreiter & Schmidhuber, 1997) architecture used already an activation-free backbone as long memory, even though inputs and gates have a standard postactivation.

Here this view is taken forward: not only the units are preactivated, but the biases become specific to each input-output pair, as the weights are. Our model indeed applies multiple biases for each signal, as was first investigated in MBA (Li et al., 2016), but with the critical difference that in DAC each unit takes as input only one activated copy of each signal, while in MBA units can use all copies. In fact, our choice has a smaller impact on the size and complexity of the network and turns out to be natural from

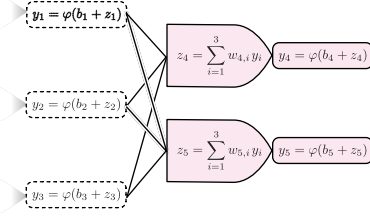


Figure 1. Standard network example. A fully connected layer consisting of 2 computational units with 3 input units. The set of in-neighbors of nodes 4 and 5 is $\mathcal{I}_4 = \mathcal{I}_5 = \{1, 2, 3\}$. The linear aggregation and nonlinear filter from (1) are denoted with bullets and rectangles, respectively. Units 4 and 5 must share the same biases b_1, b_2, b_3 in their inputs, and for this reason, the outputs y_4 and y_5 could be based on deteriorated information.

both mathematical and biological points of view.

2. From standard to DAC units

To describe this paper’s idea, we look at a neural network as a directed acyclic computational graph. We denote the set of its nodes by \mathcal{I} . If $i \in \mathcal{I}$ is a node, we denote its parents (in-neighbors) by $\mathcal{I}_i \subset \mathcal{I}$. In the *standard model* for computational units in a neural network, a bias b_i , a set of weights $w_{i,j}$ for $j \in \mathcal{I}_i$ and a nonlinearity φ_i are associated with every node i .

Remark 2.1. In this paper, φ_i is always $\varphi = \text{ReLU}$. However, using ReLU is not strictly necessary, see Section 9 on possible future developments.

The network flow in the standard model can be described in terms of computational units updating node i ’s value y_i by applying a nonlinear filter, *activation \circ bias*, to some information linearly aggregated from node i ’s parents:

$$\begin{cases} z_i = \sum_{j \in \mathcal{I}_i} w_{i,j} y_j & \text{linear aggregation} \\ y_i = \varphi(b_i + z_i) & \text{nonlinear filter} \end{cases} \quad (1)$$

Figure 1 exhibits this point of view, also emphasizing that the values in parent nodes (white boxes) are often themselves filtered with biases and ReLU. For each parent node $i = 1, 2, 3$, the bias b_i is uniquely determined. Children nodes $j = 4, 5$, cannot access z_i directly and must use the filtered versions y_i , sharing the way they are filtered. We refer to this as having *shared* biases and argue that it could result in a degradation of the information.

The direct solution to this problem is to apply the nonlinear filter with *non-shared* biases at the input of the unit, before the linear aggregation. We investigate this idea, by studying a new computational unit briefly described as *linearity \circ*

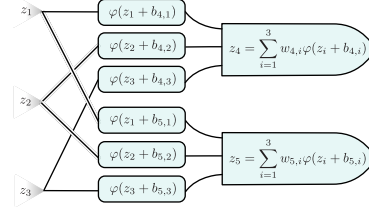


Figure 2. DAC network example: the same network of Figure 1 with standard units replaced by DAC units. The input biases b_1, b_2, b_3 , contributing to the output values z_4 and z_5 , now depend also on the output nodes 4, 5. We call this feature *non-shared* biases because it allows DAC units sharing the same input to use different (*non-shared*) thresholds instead of a single (*shared*) input bias.

(*activation \circ non-shared biases*):

$$\begin{cases} y_{i,j} = \varphi(b_{i,j} + z_j) & \text{nonlinear filter} \\ z_i = \sum_{j \in \mathcal{I}_i} w_{i,j} y_{i,j} & \text{linear aggregation} \end{cases} \quad (2)$$

The proposed extension (2) of the artificial neuron also reflects a recent shift in the understanding of the biological neuron towards a model that incorporates *active dendrites* (Larkum, 2022; Magee, 2000). Active dendrites perform a local nonlinear signal modulation before integration at the soma level. Since the biases $b_{i,j}$ in the nonlinear filter in (2) can depend on both input and output nodes, that is, on the edges of the graph, and since these edges correspond to dendrites in biological neurons, we call this new computational unit a *Dendrite-Activated Connection* (DAC) unit. See Section A for more details on biological inspiration.

One can view DAC as a preactivated unit with multiple *non-shared* input biases, meaning that DAC units sharing the same inputs can filter them with different nonlinearity thresholds, see Figure 2.

Remark 2.2. In a DAC unit, it is crucial for the filter to depend on both the input and the output nodes (*non-shared* biases), and not only on the input node (*shared* biases). In fact, if one considers a plain multilayer perceptron, the recursed equation for standard units gives:

$$y_i = \varphi \left(b_i + \sum_{j \in \mathcal{I}_i} w_{i,j} \varphi \left(b_j + \sum_{k \in \mathcal{I}_j} w_{j,k} \varphi(\dots) \right) \right). \quad (3)$$

If one uses preactivation instead of the usual activation of the output, the same equation simply becomes:

$$z_i = \sum_{j \in \mathcal{I}_i} w_{i,j} \varphi \left(b_j + \sum_{k \in \mathcal{I}_j} w_{j,k} \varphi(\dots) \right). \quad (4)$$

Without changing anything else, the modification is only formal, and the resulting network performs more or less the same operations, as can be seen by comparing the right-hand

sides of the above equations (the few differences are at the beginning and at the end of the network). A very natural extension is to make the change $b_j \rightarrow b_{i,j}$, allowing the bias to depend also on the unit i , as in (2).

Remark 2.3. The change $b_j \rightarrow b_{i,j}$ roughly doubles the number of parameters. However, when it is reasonable to assume that some input nodes carry similar information, biases can (and should) be *partially shared*. For instance, in a convolutional layer the features are position equivariant, and one should make the biases depend only on input channel and output kernel, see Section 6.

3. Related work

The multi-bias activation (MBA) from (Li et al., 2016) is by far the model most similar to DAC. MBA replicates K times the input features z_j , applies a different bias parameter $b_j^{(k)}$ to each of them, filters them with ReLU, and then computes a linear combination over j and k for every output node i :

$$z_i = \sum_{j \in \mathcal{I}_i} \sum_{k=1}^K w_{i,j,k} \varphi(b_j^{(k)} + z_j). \quad (5)$$

Equation (5) is very similar to DAC equation (2), and in fact, DAC can be obtained from MBA with suitable constraints on $w_{i,j,k}$. In particular, one needs to choose K equal to the number of units in the layer to which i belongs, and then let $w_{i,j,k} = \delta_{i,k} w_{i,j}$, and $b_j^{(i)} = b_{i,j}$, so that:

$$\begin{aligned} \sum_{k=1}^K w_{i,j,k} \varphi(b_j^{(k)} + z_j) &= \sum_{k=1}^K \delta_{i,k} w_{i,j} \varphi(b_j^{(k)} + z_j) \\ &= w_{i,j} \varphi(b_j^{(i)} + z_j) = w_{i,j} \varphi(b_{i,j} + z_j). \end{aligned}$$

However, notice how in (5) the preactivation biases do not depend explicitly on the output i , and how the number of parameters and computations are increased K -fold; see also Remark B.1 on a geometric interpretation of an MBA layer. Squeeze MBA (Fang et al., 2019) is a variation of MBA that still shares biases among outputs but tweaks the network structure to partially reduce the number of parameters.

Other approaches to mitigate the loss of information intrinsic in the ReLU activation, such as Maxout networks (Goodfellow et al., 2013), adaptive piecewise linear activation functions (Agostinelli et al., 2015), Concatenated ReLU (Shang et al., 2016), and Activation ensembles (Klabjan & Harmon, 2019), generalize the activation function by using multiple biases (among other parameters) but they all maintain a single nonlinear filtered output per node.

There are also ways to design a network that *inherently* mitigate or avoid the ReLU loss of information. ResNet v2 architecture (He et al., 2016b) keeps the information backbone free of nonlinearities that are only on residual branches

(with preactivation). All the nonlinear blocks take their inputs from the backbone, so each input is the pure linear sum of all the previous nonlinear branches. ConvNeXt (Liu et al., 2022) not only uses the same linear backbone as above, but then applies depthwise convolutions, which were brought to popularity by (Chollet, 2017) and are common to other recent successful architectures. In depthwise convolutions, every input channel is unique to one output kernel: this is a simple solution to avoid sharing biases, though the consequent low capacity requires that depthwise convolutions are used together with other types of layers that will typically have shared biases.

Finally, various forms of input preactivation originating from biological dendrites can be seen in works such as (Li et al., 2020; Jiang et al., 2015; Wu et al., 2018; Iyer et al., 2022). However, these papers address issues unrelated to the degradation of signals caused by ReLU and thus employ a vastly different approach to preactivation than DAC.

4. Geometric interpretation

DAC preactivation has an interesting geometric interpretation, fully described in Section B. We provide here only a very concise description. A fully connected DAC layer $\hat{z} : \mathbb{R}^m \rightarrow \mathbb{R}^n$ factorizes as $\hat{z} = \mathbf{p}_w \circ \hat{z}_b$:

$$\begin{array}{ccc} \mathbb{R}^m & \xrightarrow{\hat{z}} & \mathbb{R}^n = \text{Span}\{\mathbf{w}_1, \dots, \mathbf{w}_n\} \\ \hat{z}_b \downarrow & \nearrow \mathbf{p}_w & \\ \underbrace{\mathbb{R}^m \times \dots \times \mathbb{R}^m}_{n \text{ times}} & \xrightarrow{\otimes} & \underbrace{\mathbb{R}^m \otimes \dots \otimes \mathbb{R}^m}_{n \text{ times}} \end{array} \quad (6)$$

In (6), \hat{z}_b is a nonlinear embedding into a higher (unless $n = 1$) dimensional space, depending only on DAC biases and not on weights, and \mathbf{p}_w is a multilinear projection, depending only on weights and not on DAC biases.

Thus, DAC preactivation can be seen as an intermediate step preserving or increasing the dimension. This is a feature that can improve the approximation efficiency. In support of this claim, we provide two examples. In Figure 3a, a binary classification problem that cannot be solved by a standard layer $\mathbb{R}^2 \rightarrow \mathbb{R}$, but can be solved by its DAC counterpart, thanks to the intermediate embedding step maintaining the input dimension. In Figure 3b, a DAC layer $\mathbb{R}^2 \rightarrow \mathbb{R}^2$ can separate a non-linearly separable dataset thanks to the intermediate embedding doubling the input dimension.

5. Additional DAC features

Last and first layers. Consider the last layer of a plain multilayer network with ReLU activations: with standard units, one would expect a ReLU activation also at the output of the very last layer, but this is typically not desired, as

Dendrite-Activated Connection

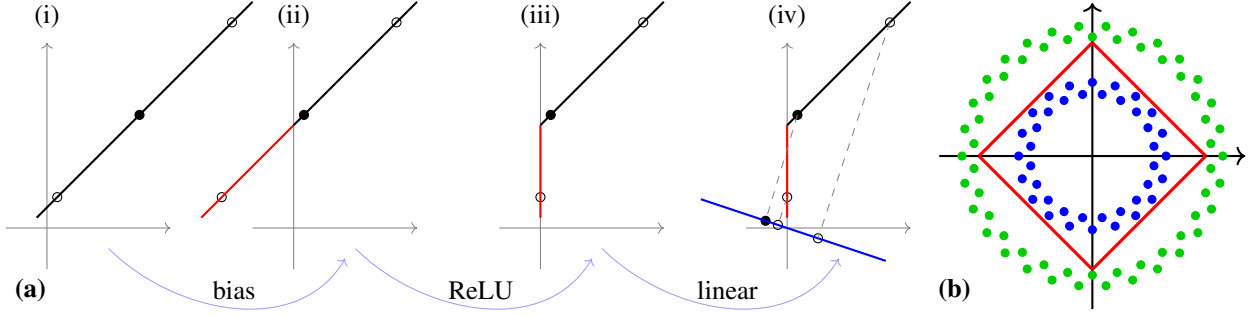


Figure 3. (a). A DAC one-layer $f : \mathbb{R}^2 \rightarrow \mathbb{R}$ can separate points that are not linearly separable. (i) Black and white points are not linearly separable. (ii) DAC can learn a translation (DAC biases) that moves the leftmost point to the second quadrant (red line). (iii) ReLU projects all points in the second quadrant onto the vertical axis (red line), making the dataset linearly separable. (iv) DAC can now learn a direction (blue line) onto which to project the dataset. The black point is now separated from the white points. (b). The combination of a DAC layer $f : \mathbb{R}^2 \rightarrow \mathbb{R}^2$ and a linear layer $g : \mathbb{R}^2 \rightarrow \mathbb{R}$ can separate the blue from the green points. In fact, let $[f(x)]_i = \sum_{j=1,2} w_{ij} \varphi(b_{ij} + x_j)$ with φ denoting ReLU, then it is enough to set $w_{1j} = 1$, $b_{1j} = 1$, $b_{2j} = 0$ and $g(y) = y_1 - 2y_2 - 1$ to get $g(f(x)) = \varphi(1 + x_1) + \varphi(1 + x_2) - 2\varphi(x_1) - 2\varphi(x_2) - 1$, which is positive and equals $1 - |x_1| - |x_2|$ inside the red square and is negative outside. On the contrary, it is easy to see that if f was a standard fully connected layer, then for all choices of f and g the set where $g(f(x)) \geq 0$ would always be unbounded or empty.

the output of the last layer must be as much informative as possible, and of the right type to be fed into the loss function (i.e. logits for the cross-entropy). So one usually has to remove that last activation, which, using DAC units, would not have existed in the first place. Here the preactivation of DAC seems more natural.

Symmetrically, consider the first layer of a similar network: with standard units, it would not make sense to filter the input nodes with ReLU, with or without some bias. Nevertheless, with DAC units, it is instead very reasonable to apply the nonlinearity to the input nodes, because the bias used to filter them can depend on the output (i.e. on the unit), and it is not completely unlikely that different units in the first layer might benefit from tailored filtering of the input. Here DAC multi-biases could be more capable of exploiting feature diversities of the inputs (this is also one of the main arguments in MBA (Li et al., 2016)).

Input replication. Filtering the input as just described might be even more useful if the input is replicated multiple times. Consider the toy example of a one-dimensional input x and a shallow network with only one layer of one unit aiming at approximating some function $f : \mathbb{R} \rightarrow \mathbb{R}$. A DAC fully connected layer with one unit ‘0’ and input replicated n times $\bar{x} = (x, x, \dots, x)$ gives:

$$\hat{f}_{\text{DAC}}(\bar{x}) = \sum_{j=1}^n w_{0,j} \varphi(b_{0,j} + x), \quad (7)$$

which is a universal approximator of a large class of functions $\mathbb{R} \rightarrow \mathbb{R}$, for $n \rightarrow \infty$ (later we prove that \hat{f}_{DAC} is a universal approximator of $C^0([-1, 1])$, see Theorem 8.1 in Section 8, and also Remark D.2).

On the other hand, a standard fully connected layer with replicated inputs and one unit would give:

$$\hat{f}_{\text{std}}(\bar{x}) = \varphi\left(b_0 + \sum_{j=1}^n w_{0,j} x\right) = \varphi(b_0 + \tilde{w}_0 x),$$

regardless of n . To gain expressivity with the standard connection we can add a hidden layer with n units (with or without replicated inputs is the same), obtaining:

$$\hat{f}_{2 \times \text{std}}(\bar{x}) = \varphi\left(b_0 + \sum_{j=1}^n w_{0,j} \varphi(b_j + \tilde{w}_j x)\right).$$

To show that $\hat{f}_{2 \times \text{std}}$ has a representation power similar to \hat{f}_{DAC} , we put $\tilde{w}_{0,j} = w_{0,j} |\tilde{w}_j|$ and $\tilde{b}_j = b_j / |\tilde{w}_j|$ in the above expression, which gives:

$$\hat{f}_{2 \times \text{std}}(\bar{x}) = \varphi\left(b_0 + \sum_{j=1}^n \tilde{w}_{0,j} \varphi(\tilde{b}_j + \text{sign}(\tilde{w}_j) x)\right).$$

Thus, in this toy problem of approximating a function $f : \mathbb{R} \rightarrow \mathbb{R}$, one needs a two-layers standard network to get a representation power similar to a single-layer DAC network.

Input replication inside the computational graph. Input replication in a DAC unit corresponds to different dendrites of the same downward neuron being connected to different branches of the axon of the same upward neuron. Biologically, given the complexity of dendrite activation, this cannot be excluded as a possibility, see Section A. This suggests that input replication could be useful at any node in the computational graph, not only on its inputs.

A thorough empirical analysis of the effects of replication on DAC performance would first require a baseline without

replication. For this reason, and because this is the first paper on the DAC paradigm, we have decided to not use replication in the experiments described in Section 7. We leave this analysis to future work, see Section 9.

6. Methods

While DAC theory has been detailed in the previous sections, here we delve into the implementation details, model efficiency and other practical considerations, starting with the application to convolutional layers.

The formula for the DAC version of a 2D convolutional layer is the following:

$$\psi \left(b_i + \sum_{a,b=-l}^l \sum_{j=1}^m w_{a,b,i,j} \varphi(b_{i,j} + y_{h+a,k+b,j}) \right), \quad (8)$$

where $L = 2l + 1$ is the kernel size, $i \in [n]$ is the output kernel, $j \in [m]$ is the input channel, (h, k) varies in the set of coordinates of the output and where ψ is an optional output activation, b_i is an optional output bias, φ is the ReLU input activation and $b_{i,j}$ are the DAC input biases. When stacking consecutive DAC layers, ψ and b_i will typically not be used, but they might in general be needed, for example, if the subsequent operation is a global average pooling. In its most general form, the DAC biases could take the form $b_{a,b,i,j}$ depending on the channel, kernel and position in the kernel, but in this paper we opted for one single DAC bias $b_{i,j}$ for every input channel and output kernel, as outlined in Remark 2.3. An analogous decision was taken also in MBA (Li et al., 2016), where the biases depend only on the input channel j and the duplication index but not on a and b . The DAC version of a fully connected layer can be simply obtained from (8) by setting $h = k = l = 0$.

6.1. Model size and efficiency

In this section, we estimate the increase in the number of parameters and floating point operations (FLOPs) for a forward pass, when using DAC layers. The use of FLOPs as an effective measure of efficiency has been advocated in (Schwartz et al., 2020). Compare the DAC version of a 2D convolutional layer in (8) with the function computed by the standard layer:

$$\psi \left(b_i + \sum_{a,b=-l}^l \sum_{j=1}^m w_{a,b,i,j} y_{h+a,k+b,j} \right). \quad (9)$$

The parameters per unit are $mL^2 + m + 1$ for DAC, against $mL^2 + 1$ for the standard case, with a relative increase factor of at most $1 + L^{-2}$. In the common case of 3×3 convolutions, this corresponds to about +11%. In the special case of the fully connected layers and 1×1 convolutions, $L = 1$, so the parameters number approximately doubles.

For the FLOPs calculation, we will follow the convention used in the analysis of standard layers that the computational cost of the activation functions can be safely ignored: despite the large number of activations involved in the DAC paradigm, it is still fine to ignore the activation costs since we consider only the ReLU activation, that requires no expensive calculations on any architecture. However, this might need to be amended in case of other, more costly, activation functions in the dendrites.

The FLOPs per unit in the standard case (9) are mL^2 multiplications and mL^2 additions. If the output shape is $s \times t$, this yields $2mL^2st$ operations per output channel. For the DAC convolution (8), we notice that, since the biases $b_{i,j}$ do not depend on the particular kernel position (a, b) , it is possible to *cache* the results of the initial activations $\varphi(b_{i,j} + y_{\cdot,\cdot,j})$. This requires mst additions per output channel (assuming for simplicity that the input shape is also $s \times t$), yielding a relative increase factor of $1 + 0.5L^{-2}$, corresponding to a +5.5% for 3×3 convolutions and +50% for 1×1 convolutions and fully connected layers.

6.2. Implementation issues

DAC architectures can be easily implemented on modern deep learning platforms using standard layers. Unfortunately, such a high-level approach in practice results in a memory footprint and computation time that are much higher than what one would expect from the estimates of the previous section.

In fact one needs to replicate the output y of the preceding layer for each of the $i \in [n]$ units/kernels of the current layer, then apply ReLU using a different bias for each input channel/output unit combination, before applying the usual layer calculations separately to each replica block, to generate the output units.

For fully connected layers we used standard matrix multiplications after reshaping the replicated input in the appropriate manner. For convolutions, using TensorFlow, we exploited the *grouping* feature of the `Conv2D` layers, to operate the convolution separately on each of the replicated inputs. This allowed us to use a single layer to handle all the convolutions at once, saving a lot of computational time as the *grouping* feature is implemented at a low level. Notice that this high-level implementation is similar to the one described in MBA (Li et al., 2016), the only difference being that in that model there is no grouping and the resulting convolution kernel is much larger.

Despite the likely optimality of this formulation among high-level approaches, the time and memory footprint during training are about 10 times higher than the standard networks. The situation is somewhat better in the case of the forward calculation, but still far from the expected effi-

ciency.

At a low level, operations such as convolutions and matrix multiplications are implemented with parallel programming, with many units that share access to parameters, inputs, and cached partial results. If a DAC layer could be implemented and optimized at that level, there would be no need to store all the n replica of the inputs at the same time, and each extra addition and ReLU $y_{i,j} = \varphi(b_{i,j} + z_j)$ could be performed just before the corresponding multiplication $w_{i,j} \cdot y_{i,j}$, arguably yielding much better performances. Such a low-level implementation is outside the scope of this paper and is planned as a possible future development, see Section 9.

6.3. Backpropagation

To write the backpropagation equations, we restrict ourselves to a fully connected multi-layer plain architecture and compute derivatives of some loss E with respect to the parameters. Let y_i , $w_{i,j}$ and $b_{i,j}$ denote the outputs, weights, and DAC biases of some layer k , and m , y_j^\diamond the number of units and outputs of layer $k - 1$. Then $y_i = \sum_{j=1}^m w_{i,j} \varphi(b_{i,j} + y_j^\diamond)$, and we get

$$\begin{cases} \frac{\partial E}{\partial w_{i,j}} = \varphi(b_{i,j} + y_j^\diamond) \frac{\partial E}{\partial y_i} \\ \frac{\partial E}{\partial b_{i,j}} = w_{i,j} \varphi'(b_{i,j} + y_j^\diamond) \frac{\partial E}{\partial y_i} \\ \frac{\partial E}{\partial y_i} = \sum_{l=1}^n w_{l,i}^* \varphi'(b_{l,i}^* + y_i) \frac{\partial E}{\partial y_l^*} \end{cases}$$

where n , $w_{l,i}^*$, $b_{l,i}^*$ and y_l^* are the number of units, weights, DAC biases and outputs of layer $k + 1$.

For a non-DAC architecture, with shared biases, $\varphi'(b_i^* + y_i)$ in the last equation would not depend on l and could be taken out of the sum, yielding a unique 0-1 factor regulating the entire derivative. Hence DAC allows for finer, granular masking of the different contributions to the gradient.

6.4. DAC ResNet architecture

For our experiments, we used the original non-bottleneck ResNet architectures (He et al., 2016a;b), where we replaced all the 3×3 convolutions with DAC versions (8) without output activation ψ and bias b_i . Everywhere convolutions were preceded by batch normalization and ReLU, we removed the trainable shift parameter β of the batch normalization and the activation (because DAC preactivation includes both).

In the case of ResNet v1, this has the collateral effect of moving the activation from the information backbone to the residual branch. This implies that DAC turns ResNet v1 into something similar to the ResNet v2 architecture, but with DAC biases instead of regular biases, and with the batch normalization layers moved after the convolutions. Apart from the biases, this is the ReLU-only preactivation that was tested in (He et al., 2016b), Fig. 4(d).

Again in the case of ResNet v1, after the last residual block and before the global average pooling, we added a traditional bias layer and a ReLU activation, since they were removed from the residual block output and no DAC layer followed.

7. Experiments and results

We first evaluate our method on a ResNet architecture for the CIFAR-10 and CIFAR-100 datasets (Krizhevsky, A. and Nair, V. and Hinton, G., 2009). Both datasets consist of 50k training images and 10k test images, divided into 10 and 100 different classes, respectively. We replicate each experiment 5 times, using a 5-fold cross-validation scheme for splitting the 50k training dataset into a 10k validation set and a 40k training set.

7.1. Implementation details

Since there is no established ResNet implementation for CIFAR-10 and CIFAR-100, we choose the architecture proposed in the original papers (He et al., 2016a;b). Our implementation can be found in the supplementary material, and will appear on GitHub. To our knowledge, it is the most faithful public Keras implementation of these architectures.

We experiment with 20, 32, 44, and 56 layers ($n = 3, 5, 7, 9$) both with the v1 postactivated (He et al., 2016a) architecture and the v2 preactivated (He et al., 2016b) architecture. We do not use bottleneck architectures since, according to the authors, they should give a significant improvement only for deeper networks (see also Remark 7.1 below). We train with the same settings, hyperparameters and data augmentation of the cited papers, except that we choose L²-regularization of kernel weights, over weight decay of all parameters used by the authors. Regularization coefficients are fine-tuned to $2 \cdot 10^{-4}$ for CIFAR-10 and $3 \cdot 10^{-4}$ for CIFAR-100, which we find to be optimal for baseline ResNets. The same coefficients are used for the DAC versions, without further optimization. In order to explore the possibility of improvements with lower learning rates, we add an extra window of 16k iterations at the end of the regular 64k schedule, with a further 10-fold learning rate cut.

Next, we train the corresponding DAC ResNet architectures, with identical settings and hyperparameters as for baseline networks. For the DAC input biases, we adopt the same choices as the baseline biases, i.e. initialization to zero and no regularization.

Remark 7.1. Bottleneck architectures would present an additional difficulty: their heavy use of 1×1 convolutions results in a large increase in complexity when converted into DAC (see Section 6.1). This suggests the need to tweak channels and other hyperparameters to get a meaningful comparison, and this is beyond the scope of this work.

Dendrite-Activated Connection

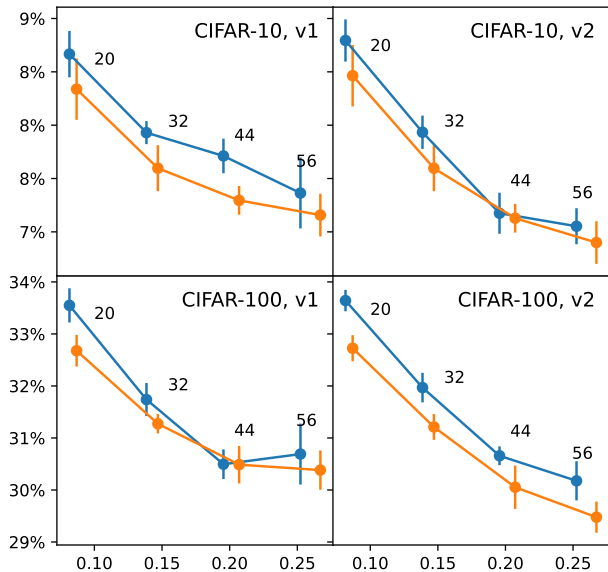


Figure 4. Compared performances of ResNet baseline (blue) and DAC (orange) networks on CIFAR-10 (top) and CIFAR-100 (bottom) with architectures v1 (left) and v2 (right). Floating numbers are the layers count. Test error (vertical axis) is averaged over the 5 replicates and over 5 epochs centered on the best epoch on the validation dataset, see Section C. Error bars are 2 standard errors wide. Complexity (horizontal axis) is measured in GFLOPs per forward pass. DAC networks of the same number of layers have about 6% more FLOPs than the baseline, but this cannot account for their performance improvement against it.

7.2. Results

Figure 4 compares the baseline and DAC networks according to a robust estimate of the test error. It is apparent that DAC networks are consistently better than the baseline, and that this cannot be explained merely by the small increase in complexity, because most of the orange dots are well below the blue lines connecting baseline networks of increasing complexity.

Table 1 summarizes a simpler statistics, namely the least test error rate (minimum over the epochs of the average of the 5 replicates) as is usually reported in the literature. Both the figure and the table outline the same picture: DAC networks show a significant performance improvement in almost all versions and benchmark datasets. They sometimes outperform the corresponding baselines even with fewer layers. Figure 5 shows the training and test evolution plots.

Imagenette and Imgewoof. Imagenette and Imgewoof (Jeremy Howard, 2019) are two subsets of ImageNet often used for model benchmarking because they provide a simple and faster alternative to ImageNet while preserving many of the inherent challenges. Imagenette is a subset of 10 well-distinguished classes, while Imgewoof consists of

Table 1. Comparison of test errors on CIFAR-10 and CIFAR-100.

Layers	CIFAR-10, v1		CIFAR-10, v2	
	Base	DAC	Base	DAC
20	8.64%	8.27%	8.73%	8.32%
32	7.90%	7.56%	7.84%	7.55%
44	7.68%	7.26%	7.14%	7.09%
56	7.33%	7.12%	7.01%	6.88%

Layers	CIFAR-100, v1		CIFAR-100, v2	
	Base	DAC	Base	DAC
20	33.50%	32.53%	33.49%	32.62%
32	31.65%	31.09%	31.79%	31.04%
44	30.39%	30.42%	30.50%	29.92%
56	30.53%	30.32%	29.89%	29.31%

Table 2. Comparison of test errors on Imagenette and Imgewoof.

Layers	Imagenette, v1		Imagenette, v2	
	Base	DAC	Base	DAC
20	13.41%	11.88%	11.97%	11.78%
32	13.13%	11.75%	11.40%	11.27%

Layers	Imgewoof, v1		Imgewoof, v2	
	Base	DAC	Base	DAC
20	23.19%	22.60%	22.61%	21.70%
32	23.05%	21.32%	21.75%	20.65%

GFLOPs	0.509	0.542	0.509	0.542
	0.865	0.918	0.865	0.918

10 classes very similar to each other because they picture 10 different dog breeds. For each dataset, we opt for its 160 pixels version (that is, the shortest side is resized to 160 pixels, with the aspect ratio maintained), which is further processed to a final size of 80×80 pixels.

We use the same settings, hyperparameters, data augmentation, and cross-validation policy as for CIFAR-10, adapting only for the smaller cardinality of the datasets. The regularization coefficient is again optimized on baseline networks, yielding $2 \cdot 10^{-4}$ as it is for CIFAR-10. We train baseline and DAC ResNet with 20 and 32 layers.

Table 2 shows the resulting test error rates (minimum over the epochs of the average of the 5 replicates). The performances of the baseline networks are in accordance with the typical values for networks of similar complexity from the literature. DAC networks outperform baseline networks even with fewer layers, and the improvement is higher than in the case of CIFAR-10 and CIFAR-100.

Ablation study. Since DAC features both preactivation and multiple biases, we test DAC with preactivation but without multiple biases (sDAC), on ResNet v1 and v2 architectures, with 20 layers, both on CIFAR-10 and CIFAR-100. We find that these models perform similarly to the baseline

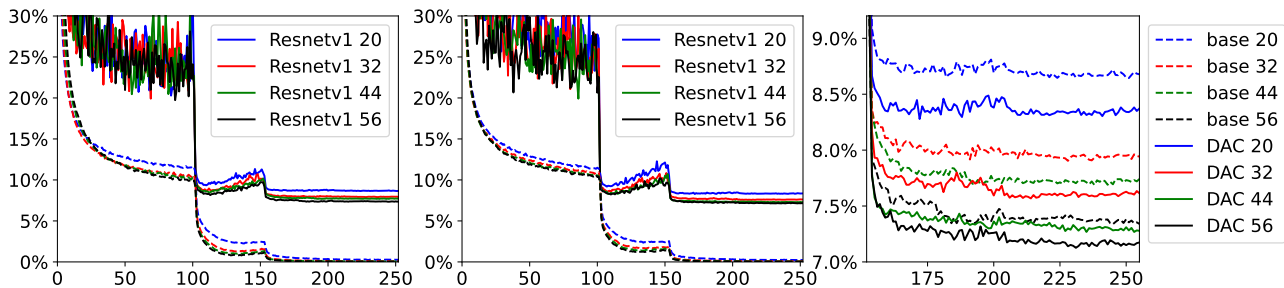


Figure 5. Training evolution for ResNet v1 baseline and DAC networks for CIFAR-10 dataset (left, center). Training error in dashed lines, test error in continuous lines. In the central part of the training, there is an accentuated overfitting phenomenon, probably due to the choice of hyperparameters, including the high amount of regularization injected. Despite this phenomenon, the final performances correspond to those of the original papers (He et al., 2016a;b), as can be appreciated from the zoom of the test error on the last 100 epochs (right).

model, and clearly worse than DAC, with the following differences in test accuracy (positive values mean sDAC is better).

test accuracy	sDAC – base		sDAC – DAC	
	v1	v2	v1	v2
CIFAR-10	-0.13%	0.08%	-0.45%	-0.19%
CIFAR-100	-0.13%	0.10%	-1.06%	-0.86%

This was expected for plain networks since we motivated in Remark 2.2 that in that setting preactivation without multiple biases should be very similar to postactivation. Our experiment confirms this behavior also for small ResNet networks.

We also consider the idea of a multi-bias but not preactivated version of DAC, and we conclude that the natural way to realize it is the MBA layer (Li et al., 2016), see Section 3. We design mDAC by modifying the DAC version of the ResNet v2 architecture, inserting MBA+convolution blocks where DAC layers had been. We test mDAC on CIFAR-100 with multiplication factors $K = 2, 4, 8$. The results are intermediate between the baseline and DAC, even if mDAC models are about K times larger. We believe that mDAC would need a specific tuning of the learning rate schedule to get better performances, and DAC in this respect seems superior, as it works well without tuning.

8. Universal approximation

Following the idea proposed in (Cybenko, 1989) and the direct construction in (Chen et al., 1992) we prove the following density result, see also (Park et al., 2021).

Theorem 8.1 (Universal approximation for DAC). *Let \mathcal{G}_d be the set of functions $g : [-1, 1]^d \rightarrow \mathbb{R}$ representable by a DAC fully connected neural network with ReLU preactivation and d layers, for $d \geq 1$. Then \mathcal{G}_d is dense in $C^0([-1, 1]^d)$. In particular, for every function $f \in C^0([-1, 1]^d)$ and every $\varepsilon > 0$, there exists a ReLU fully connected DAC neural network $g \in \mathcal{G}_d$ with d DAC layers*

such that $\|f - g\|_\infty := \sup_{\mathbf{x}} |f(\mathbf{x}) - g(\mathbf{x})| < \varepsilon$. Moreover, for $d \geq 2$, g is sparse, in the sense that there exists $k := k(\varepsilon, f) \in \mathbb{N}$ such that layer $l = 1, 2, \dots, d - 1$ of g has $2k + d - l$ units, each with no more than 4 input nodes.

Proof. For the complete proof, see Section D. Here we give a general idea, that starts with the fact that ReLU can be used to build a narrow spike function. From this, we build a family of densities $\psi_{d,\delta} \in \mathcal{G}_d$ that can approximate the Dirac delta in dimension d . By the approximation property of the convolution, the operator $T_{d,\delta}(f) := f * \psi_{d,\delta}$ approximates the identity on $C^0([-1, 1]^d)$ when δ is small. Since the convolution is a d -dimensional integral, one can approximate it with a sum over a finite partition of the domain, maintaining the desired accuracy by choosing an appropriate mesh size. Finally, we show that the sum itself corresponds to a DAC network that merges one subnet for each of the terms of the summation, and by induction, we obtain sharp bounds on the growth of the number of units and their input nodes. \square

Two interesting remarks follow from Theorem 8.1. First, the case $d = 1$ shows that a single-layer DAC neural network is a universal approximator in $C^0([-1, 1])$ via exploitation of the input replication, see Section 5; this feature is not shared by standard single-layer neural networks. Second, by observing that $\psi_{d,\delta}$ can also be realized as a 2-layer DAC network, one could prove a result similar to Theorem 8.1, but with a DAC network with 2 layers, regardless of d , losing the sparsity property. See Remark D.4 for more details.

9. Future work and limitations

In our opinion, the most significant limitation and potential future development of DAC is its current high-level implementation. As mentioned in Section 6.2, an efficient low-level implementation of DAC could potentially result in only a modest increase in computational complexity compared to its non-DAC counterpart (of the same order as the increase in the number of parameters). This would be the

first step towards integrating DAC into frameworks such as PyTorch and Keras, making it a standard option for layers.

Future development for DAC could include experimenting with alternative activation and postactivation functions, and compressing the network via *partially-shared* biases, see Remark 2.3. Additionally, comparing filters learned by DAC and non-DAC networks and evaluating DAC's performance on other architectures and tasks could also be examined.

Acknowledgements. Computational resources for this work were provided by [Computational Logic and Artificial Intelligence \(CLAI\) laboratory](#) of university of Chieti-Pescara. Maurizio Parton was partially funded by INdAM group GNSAGA. The authors would like to express their sincerest gratitude to Rosa Gini for her invaluable contribution to this project.

References

- Agostinelli, F., Hoffman, M., Sadowski, P., and Baldi, P. Learning Activation Functions to Improve Deep Neural Networks, April 2015. URL <http://arxiv.org/abs/1412.6830>. arXiv:1412.6830 [cs, stat].
- Chen, T., Chen, H., and Liu, R.-w. A constructive proof and an extension of cybenko's approximation theorem. In Page, C. and LePage, R. (eds.), *Computing Science and Statistics*, pp. 163–168, New York, NY, 1992. Springer New York. ISBN 978-1-4612-2856-1.
- Chollet, F. Xception: Deep Learning with Depthwise Separable Convolutions. pp. 1800–1807. IEEE Computer Society, July 2017. ISBN 978-1-5386-0457-1. doi: 10.1109/CVPR.2017.195. URL <https://www.computer.org/csdl/proceedings-article/cvpr/2017/0457b800/12OmNqFJhzG>. ISSN: 1063-6919.
- Clevert, D.-A., Unterthiner, T., and Hochreiter, S. Fast and Accurate Deep Network Learning by Exponential Linear Units (ELUs), February 2016. URL <http://arxiv.org/abs/1511.07289>. arXiv:1511.07289 [cs].
- Cybenko, G. Approximation by superpositions of a sigmoidal function. *Mathematics of control, signals and systems*, 2(4):303–314, 1989.
- Fang, L., Liu, G., Li, S., Ghamisi, P., and Benediktsson, J. A. Hyperspectral Image Classification With Squeeze Multi-bias Network. *IEEE Transactions on Geoscience and Remote Sensing*, 57(3):1291–1301, March 2019. ISSN 1558-0644. doi: 10.1109/TGRS.2018.2865953. Conference Name: IEEE Transactions on Geoscience and Remote Sensing.
- Goodfellow, I. J., Warde-Farley, D., Mirza, M., Courville, A. C., and Bengio, Y. Maxout networks. In *Proceedings of the 30th International Conference on Machine Learning, ICML 2013, Atlanta, GA, USA, 16-21 June 2013*, volume 28 of *JMLR Workshop and Conference Proceedings*, pp. 1319–1327. JMLR.org, 2013. URL <http://proceedings.mlr.press/v28/goodfellow13.html>.
- He, K., Zhang, X., Ren, S., and Sun, J. Deep residual learning for image recognition. In *IEEE conference on computer vision and pattern recognition*, pp. 770–778, 2016a.
- He, K., Zhang, X., Ren, S., and Sun, J. Identity mappings in deep residual networks. In Leibe, B., Matas, J., Sebe, N., and Welling, M. (eds.), *Computer Vision - ECCV 2016 - 14th European Conference, Amsterdam, The Netherlands, October 11-14, 2016, Proceedings, Part IV*, volume 9908 of *Lecture Notes in Computer Science*, pp. 630–645. Springer, 2016b. doi: 10.1007/978-3-319-46493-0_38. URL https://doi.org/10.1007/978-3-319-46493-0_38.
- Hochreiter, S. and Schmidhuber, J. Long short-term memory. *Neural computation*, 9(8):1735–1780, 1997.
- Iyer, A., Grewal, K., Velu, A., Souza, L. O., Forest, J., and Ahmad, S. Avoiding catastrophe: Active dendrites enable multi-task learning in dynamic environments. *Frontiers in Neurorobotics*, 16:846219, 2022. doi: 10.3389/fnbot.2022.846219. URL <https://doi.org/10.3389/fnbot.2022.846219>.
- Jeremy Howard. Imagenette and Imagewoof datasets, 2019. <https://github.com/fastai/imagenette>.
- Jiang, T., Wang, D., Ji, J., Todo, Y., and Gao, S. Single dendritic neuron with nonlinear computation capacity: A case study on XOR problem. In *2015 IEEE International Conference on Progress in Informatics and Computing (PIC)*, pp. 20–24, Dec 2015. doi: 10.1109/PIC.2015.7489802.
- Klabjan, D. and Harmon, M. Activation Ensembles for Deep Neural Networks. In *2019 IEEE International Conference on Big Data (Big Data)*, pp. 206–214, December 2019. doi: 10.1109/BigData47090.2019.9006069.
- Krizhevsky, A. and Nair, V. and Hinton, G. CIFAR-10 and CIFAR-100 datasets, 2009. <https://www.cs.toronto.edu/~kriz/cifar.html>.
- Larkum, M. E. Are Dendrites Conceptually Useful? *Neuroscience*, 489:4–14, May 2022. ISSN 03064522. doi: 10.1016/j.neuroscience.2022.03.008.

- Li, H., Ouyang, W., and Wang, X. Multi-bias non-linear activation in deep neural networks. In Balcan, M. and Weinberger, K. Q. (eds.), *Proceedings of the 33rd International Conference on Machine Learning, ICML 2016, New York City, NY, USA, June 19-24, 2016*, volume 48 of *JMLR Workshop and Conference Proceedings*, pp. 221–229. JMLR.org, 2016. URL <http://proceedings.mlr.press/v48/lial16.html>.
- Li, X., Tang, J., Zhang, Q., Gao, B., Yang, J. J., Yang, J. J., Song, S., Wu, W., Zhang, W., Yao, P., Deng, N., Deng, L., Xie, Y., Qian, H., and Wu, H. Power-efficient neural network with artificial dendrites. *Nature nanotechnology*, 15(9):776–782, September 2020. ISSN 1748-3387. doi: 10.1038/s41565-020-0722-5. URL <https://doi.org/10.1038/s41565-020-0722-5>.
- Liu, Z., Mao, H., Wu, C.-Y., Feichtenhofer, C., Darrell, T., and Xie, S. A ConvNet for the 2020s. pp. 11976–11986, 2022. URL https://openaccess.thecvf.com/content/CVPR2022/html/Liu_A_ConvNet_for_the_2020s_CVPR_2022_paper.html.
- Maas, A. L., Hannun, A. Y., and Ng, A. Y. Rectifier Non-linearities Improve Neural Network Acoustic Models. In *Proc. icml*, volume 30, pp. 3. Atlanta, Georgia, USA, 2013.
- Magee, J. C. Dendritic integration of excitatory synaptic input. *Nature Reviews Neuroscience*, 1(3):181–190, 2000.
- Park, S., Yun, C., Lee, J., and Shin, J. Minimum width for universal approximation. In *International Conference on Learning Representations*, 2021. URL <https://openreview.net/forum?id=O-XJwyoIF-k>.
- Poirazi, P. and Papoutsis, A. Illuminating dendritic function with computational models. *Nature Reviews Neuroscience*, 21(6):303–321, 2020. ISSN 1471-003X, 1471-0048. doi: 10.1038/s41583-020-0301-7. URL <http://www.nature.com/articles/s41583-020-0301-7>.
- Schwartz, R., Dodge, J., Smith, N. A., and Etzioni, O. Green ai. *Commun. ACM*, 63(12):54–63, nov 2020. ISSN 0001-0782. doi: 10.1145/3381831. URL <https://doi.org/10.1145/3381831>.
- Shang, W., Sohn, K., Almeida, D., and Lee, H. Understanding and improving convolutional neural networks via concatenated rectified linear units. In Balcan, M. F. and Weinberger, K. Q. (eds.), *Proceedings of The 33rd International Conference on Machine Learning*, volume 48 of *Proceedings of Machine Learning Research*, pp. 2217–2225, New York, New York, USA, 20–22 Jun 2016. PMLR. URL <https://proceedings.mlr.press/v48/shang16.html>.
- Sinha, M. and Narayanan, R. Active dendrites and local field potentials: Biophysical mechanisms and computational explorations. *Neuroscience*, 489:111–142, 2022. ISSN 0306-4522. doi: <https://doi.org/10.1016/j.neuroscience.2021.08.035>. URL <https://www.sciencedirect.com/science/article/pii/S0306452221004504>. Dendritic contributions to biological and artificial computations.
- Wu, X., Liu, X., Li, W., and Wu, Q. Improved expressivity through dendritic neural networks. In Bengio, S., Wallach, H. M., Larochelle, H., Grauman, K., Cesa-Bianchi, N., and Garnett, R. (eds.), *Advances in Neural Information Processing Systems 31: Annual Conference on Neural Information Processing Systems 2018, NeurIPS 2018, December 3-8, 2018, Montréal, Canada*, pp. 8068–8079, 2018. URL <https://proceedings.neurips.cc/paper/2018/hash/e32c51ad39723ee92b285b362c916ca7-Abstract.html>.

A. Biological inspiration

The proposed extension of the artificial neuron also reflects to some extent a recent shift in the understanding of the biological neuron. In fact, the early soma-centric representation of the neuron today has been discarded in favor of a more realistic and complex model that incorporates *active* dendrites (Larkum, 2022; Sinha & Narayanan, 2022).

A typical biological neuron consists of many input branches called dendrites, a main body called soma, and the axon, which branches at its end in many terminals, where synapses connect to the dendrites of other neurons. The input signals originate in the dendrites, flow through the soma, and are integrated into the region of the soma where the axon connects, and if a specific threshold is reached, the neuron fires its signal down the axon, to the synapses.

Until some years ago, the biological neuron model was soma-centric and essentially modeled by a point neuron where dendrites simply pass the signals, and all elaboration happens at the soma. This elementary representation was the inspiration of the traditional perceptron in artificial neural networks.

Current biological models are more complicated and the central role of dendrites in signal modulation is better understood (Poirazi & Papoutsis, 2020). Dendrites in fact present voltage-gated ion channels (Larkum, 2022) able to produce local electrical events termed dendritic spikes. Dendrites actually present at least four groups of ion channels (Sinha & Narayanan, 2022): the synaptic receptors, activated by neurotransmitters, the passive leak channels, and the active subthreshold ion channels, able to produce transmembrane currents also when the threshold for the action potential is not reached, and supra-threshold ion channel active when the threshold is reached. In this way, a dendrite or a group of dendrites can perform the first important local, not linear signal integration before reaching the cell axon.

B. Geometric interpretation

In a fully connected DAC layer, DAC equation (2) can be written in vectorial form. Let m, n be the number of input and output nodes, respectively. Denote by $\mathbf{z} \in \mathbb{R}^m$ the input, by $\hat{\mathbf{z}} \in \mathbb{R}^n$ the output, by $\mathbf{b}_1, \dots, \mathbf{b}_n \in \mathbb{R}^m$ the DAC biases, by $\mathbf{w}_1, \dots, \mathbf{w}_n \in \mathbb{R}^m$ the weights, by $\langle \cdot, \cdot \rangle$ the scalar product in \mathbb{R}^m and by φ component-wise ReLU. DAC equation (2) then becomes:

$$\hat{\mathbf{z}}(\mathbf{z}) = (\langle \mathbf{w}_1, \varphi(\mathbf{b}_1 + \mathbf{z}) \rangle, \dots, \langle \mathbf{w}_n, \varphi(\mathbf{b}_n + \mathbf{z}) \rangle)^T. \quad (10)$$

The preactivation in (10) has a geometric interpretation: a DAC layer $\hat{\mathbf{z}}$ factorizes as $\hat{\mathbf{z}} = \mathbf{p}_w \circ \hat{\mathbf{z}}_b$, where $\hat{\mathbf{z}}_b$ is a nonlinear embedding into a higher (unless $n = 1$) dimensional space, depending only on DAC biases and not on weights:

$$\begin{aligned} \hat{\mathbf{z}}_b : \mathbb{R}^m &\longrightarrow \overbrace{\mathbb{R}^m \times \dots \times \mathbb{R}^m}^{n \text{ times}} \\ \mathbf{z} &\longmapsto (\varphi(\mathbf{b}_1 + \mathbf{z}), \dots, \varphi(\mathbf{b}_n + \mathbf{z})) \end{aligned} \quad (11)$$

and \mathbf{p}_w is a multilinear map, depending only on weights and not on DAC biases, projecting back each of the n components of $\mathbb{R}^m \times \dots \times \mathbb{R}^m$ orthogonally onto the axes \mathbf{w}_i of $\text{Span}\{\mathbf{w}_1, \dots, \mathbf{w}_n\} \subset \mathbb{R}^m \times \dots \times \mathbb{R}^m$:

$$\begin{aligned} \mathbf{p}_w : \overbrace{\mathbb{R}^m \times \dots \times \mathbb{R}^m}^{n \text{ times}} &\longrightarrow \text{Span}\{\mathbf{w}_1, \dots, \mathbf{w}_n\} = \mathbb{R}^n \\ (\mathbf{y}_1, \dots, \mathbf{y}_n) &\longmapsto (\langle \mathbf{w}_1, \mathbf{y}_1 \rangle, \dots, \langle \mathbf{w}_n, \mathbf{y}_n \rangle)^T \end{aligned} \quad (12)$$

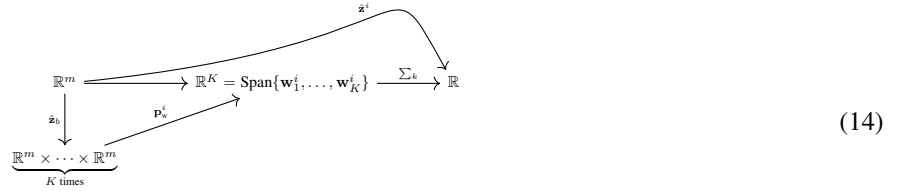
The multilinear map \mathbf{p}_w can be seen also as the corresponding linear map \mathbf{p}_w^\otimes on the tensor product $\mathbb{R}^m \otimes \dots \otimes \mathbb{R}^m$, and the whole factorization can be visualized with the commutative diagram (13):

$$\begin{array}{ccc} \mathbb{R}^m & \xrightarrow{\hat{\mathbf{z}}} & \mathbb{R}^n = \text{Span}\{\mathbf{w}_1, \dots, \mathbf{w}_n\} \\ \hat{\mathbf{z}}_b \downarrow & \nearrow \mathbf{p}_w & \uparrow \mathbf{p}_w^\otimes \\ \underbrace{\mathbb{R}^m \times \dots \times \mathbb{R}^m}_{n \text{ times}} & \xrightarrow{\otimes} & \underbrace{\mathbb{R}^m \otimes \dots \otimes \mathbb{R}^m}_{n \text{ times}} \end{array} \quad (13)$$

Thus, DAC preactivation can be seen as an intermediate step: a nonlinear embedding into a space of equal (if $n = 1$) or increased (if $n > 1$) dimension, followed by a projection. Note that a standard layer is a linear map $\mathbb{R}^m \rightarrow \mathbb{R}^n$ followed by the nonlinearity, and as such does not have a similar geometric interpretation.

In general, maintaining or increasing the dimension, before the last classification layer, can make a problem easier. In Figure 3a, we provide a toy example of a binary classification problem that cannot be solved by a standard layer $\mathbb{R}^2 \rightarrow \mathbb{R}$, but can be solved by its DAC counterpart, thanks to the intermediate embedding step maintaining the input dimension. In Figure 3b, another toy example, where a DAC layer $\mathbb{R}^2 \rightarrow \mathbb{R}^2$ can separate a dataset thanks to the intermediate embedding doubling the input dimension.

Remark B.1. A similar geometric interpretation for the MBA layer (Li et al., 2016) described in Section 3 shows why MBA is K times computationally more expensive than DAC. For a replication factor K , the embedding \hat{z}_b in (11) remains the same, with the embedding dimension $m \cdot n$ replaced by $m \cdot K$. However, this uncoupling of the embedding from the output dimension n forces an additional dependence for the remaining components of the factorization (13): the weights $w_k^i \in \mathbb{R}^m$ and the corresponding projection in (12) are now specific to each MBA unit, see Diagram (14). This means that every MBA output unit i can use all the $m \cdot K$ biases, while a DAC output unit i would see only its own m biases.



C. Error rate estimation

While we always trained for the same number of steps, we evaluated the best error rate by simulating early stopping. Let $v_{k,j}$ and $t_{k,j}$ denote the validation and test errors for replicate k and epoch j . We select the epoch m corresponding to the minimum validation error (averaging on the 5 replicates and on a moving window of 5 epochs), and then compute the average test error of the same 5 epochs and replicates:

$$m := \arg \min_i \frac{1}{25} \sum_{k=1}^5 \sum_{j=-2}^2 v_{k,i+j}, \quad \bar{T} := \frac{1}{25} \sum_{k=1}^5 \sum_{j=-2}^2 t_{k,m+j}.$$

This approach allows for evaluation of the statistical error of the estimator and it is more robust and reliable than simply taking the minimum of the test error, as in a real application one would be able to choose the early stopping on the validation set, but not on the test set.

Assuming that $t_{k,m+j} = \mu_m + \sigma Z_k + \tau Z_{k,j}$, with μ_m the true value, Z_k and $Z_{k,j}$ independent standard Gaussian noises, and σ, τ coefficients measuring randomness in replicates and epochs, the square of the standard error of \bar{T} is $\text{Var}(\bar{T}) = \frac{1}{5}\sigma^2 + \frac{1}{25}\tau^2$. Here the two terms were conservatively estimated using respectively:

$$\sigma^2 \leq \sigma^2 + \tau^2 \approx \frac{1}{4} \sum_{k=1}^5 (t_{k,m} - \bar{T})^2 \quad \text{and} \quad \frac{1}{5}\tau^2 \approx \frac{1}{4} \sum_{j=-2}^2 (t_{*,m+j} - \bar{T})^2.$$

D. Universal approximation

In this section, we follow the idea proposed in (Cybenko, 1989) and the direct construction in (Chen et al., 1992) to prove a density result for the set of functions representable by a DAC fully connected neural network. In particular, we exploit the fact that ReLU can be used to build a narrow spike function, to show that its convolutions can approximate the identity operator, and hence continuous function defined on a compact set of \mathbb{R}^d can be approximated by a DAC fully connected neural network having d DAC layers (and one replication layer, see Section 5, paragraphs on input replication), with a number of units in each layer growing at most linearly in the dimension d . This result is analogous to the one in (Park et al., 2021).

Theorem D.1 (Universal approximation for DAC). *Let \mathcal{G}_d be the set of functions $g : [-1, 1]^d \rightarrow \mathbb{R}$ representable by a DAC fully connected neural network with ReLU preactivation and d layers, for $d \geq 1$. Then \mathcal{G}_d is dense in $C^0([-1, 1]^d)$. In particular, for every function $f \in C^0([-1, 1]^d)$ and every $\varepsilon > 0$, there exist a ReLU fully connected DAC neural network $g \in \mathcal{G}_d$ with d DAC layers such that $\|f - g\|_\infty := \sup_{\mathbf{x}} |f(\mathbf{x}) - g(\mathbf{x})| < \varepsilon$. Moreover, for $d \geq 2$, g is sparse, in the sense that there exists $k := k(\varepsilon, f) \in \mathbb{N}$ such that layer $l = 1, 2, \dots, d - 1$ of g has $2k + d - l$ units with no more than 4 input nodes each.*

Proof. The general idea to prove the theorem is to first build a family of densities $\psi_{d,\delta}$ that can approximate the Dirac delta in dimension d , and show that $\psi_{d,\delta}$ is actually in \mathcal{G}_d , see (23). Then one can define the convolution operator $T_{d,\delta}(f) := f * \psi_{d,\delta}$ and show that $T_{d,\delta}$ approximates the identity on $C^0([-1, 1]^d)$ when δ is small. Since the convolution is a d -dimensional integral, one can then approximate it with a sum over a finite partition of the domain, maintaining the desired accuracy by choosing an appropriate mesh size. Finally, one shows that the sum itself corresponds to a DAC network that merges one subnet for each of the terms of the summation.

We start with the proof in the simplest case $d = 1$, which will be used for the induction in the general case.

d = 1. Consider the set \mathcal{G}_1 of functions $\mathbb{R} \rightarrow \mathbb{R}$ given by a single-layer, one unit DAC neural network, with input replication as described in Section 5 and ReLU preactivation: $g \in \mathcal{G}_1$ if:

$$g(x) = \sum_{i=1}^n w_i \varphi(b_i + x)$$

for some integer n and parameters w_i, b_i for $i = 1, \dots, n$. The aim of this paragraph is to show that \mathcal{G}_1 is dense in $C^0([-1, 1])$, giving a bound on the ‘size’ n of the DAC layer needed to approximate to some level a given function. Note that in this case there is only one unit in the layer, and n is the replication factor of the single input $x \in \mathbb{R}$.

To prove the claim one needs to find, for every continuous f and every desired accuracy ε , some $g \in \mathcal{G}_1$ such that $\|f - g\|_\infty < \varepsilon$. To do this we start by building a spike function $\psi_1 : \mathbb{R} \rightarrow \mathbb{R}$:

$$\psi_1(x) := \begin{cases} 0 & |x| \geq 1 \\ 1 - |x| & |x| < 1 \end{cases} \quad (15)$$

Note that $\psi_1 \in \mathcal{G}_1$, with the input x replicated 3 times:

$$\psi_1(x) = \varphi(-1 + x) - 2\varphi(x) + \varphi(1 + x) \in \mathcal{G}_1. \quad (16)$$

Linear rescalings of ψ_1 are also in \mathcal{G}_1 , in particular for $\delta > 0$, we introduce:

$$\psi_{1,\delta}(x) := \delta^{-1} \psi(\delta^{-1}x) = \delta^{-2} [\varphi(-\delta + x) - 2\varphi(x) + \varphi(\delta + x)]. \quad (17)$$

Notice that $\int_{-1}^1 \psi_{1,\delta}(x) dx = 1$ and $\psi_{1,\delta}(x) = 0$ for $|x| > \delta$, so if we consider the convolution operator $T_{1,\delta}(f) := f * \psi_{1,\delta}$, defined by:

$$f * \psi_{1,\delta}(x) := \int_{-1}^1 f(t) \psi_{1,\delta}(x - t) dt \quad (18)$$

then by the approximation property of the convolution, $T_{1,\delta}(f) \rightarrow f$ uniformly for $\delta \rightarrow 0$, meaning that:

$$\forall f \in C^0([-1, 1]), \forall \varepsilon > 0, \exists \delta > 0 \text{ s.t. } \|f - f * \psi_{1,\delta}\|_\infty < \varepsilon/2.$$

The next step is approximating the integral in (18) with a finite sum that happens to be an element of \mathcal{G}_1 . The integrand function $t \mapsto h(t) := f(t) \psi_{1,\delta}(x - t)$ is continuous, so there exists an integer k such that:

$$\left| \int_{-1}^1 h(t) dt - \sum_{j=1}^k h\left(\frac{2j-1}{k} - 1\right) \frac{2}{k} \right| < \varepsilon/2.$$

In principle, this k might depend on x , but since we are in a compact set, it is clear that one can choose a k that satisfies the inequality for all x . For the sake of notation simplicity, let $t_j := \frac{2j-1}{k} - 1$ and define $g(x) := \sum_{j=1}^k \frac{2}{k} h(t_j)$, yielding $\|f * \psi_{1,\delta} - g\|_\infty < \varepsilon/2$ and so $\|f - g\|_\infty < \varepsilon$ as desired.

We are only left to show that $g \in \mathcal{G}_1$. In fact, expanding the definitions of h and $\psi_{1,\delta}$, and letting $w_j := \frac{2}{k} f(t_j)\delta^{-2}$, we get:

$$g(x) = \sum_{j=1}^k \frac{2}{k} f(t_j) \psi_{1,\delta}(x - t_j) = \sum_{j=1}^k [w_j \varphi(-t_j - \delta + x) - 2w_j \varphi(-t_j + x) + w_j \varphi(-t_j + \delta + x)]. \quad (19)$$

The right side of (19) shows that $g \in \mathcal{G}_1$ with the input x replicated $3k$ times, that is, g is a single-layer, one unit DAC neural network with $3k$ (replicated) input nodes approximating f uniformly with accuracy ε . The weights and DAC biases of g are a combination of those of $\psi_{1,\delta}$ from (17) with w_j and t_j . This is explicitly written in the right-hand side of (19), where we can see that $n = 3k$, the weights are $w_j, -2w_j, w_j$ and the DAC biases are $-t_j - \delta, -t_j, -t_j + \delta$, for $j = 1, \dots, k$. This concludes the proof in the case $d = 1$.

$d \geq 2$. The first step is to build a spike function $\psi_d : \mathbb{R}^d \rightarrow \mathbb{R}$ in dimension d . As in (15), we can define:

$$\psi_d(\mathbf{x}) := \begin{cases} 0 & \|\mathbf{x}\|_1 \geq 1 \\ 1 - \|\mathbf{x}\|_1 & \|\mathbf{x}\|_1 < 1 \end{cases} \quad (20)$$

where $\|\mathbf{x}\|_1 := \sum_{j=1}^d |x_j|$. Consider $\tilde{\psi} : \mathbb{R} \times \mathbb{R}^+ \rightarrow \mathbb{R}$ defined by:

$$\tilde{\psi}(x, t) := \varphi(x - t) - 2\varphi(x) + \varphi(x + t) = (t - |x|)^+.$$

If $\mathbf{x} = (x_1, \dots, x_d)$, let $\tilde{\mathbf{x}} = (x_1, \dots, x_{d-1})$. Then:

$$\psi_d(\mathbf{x}) = \left(1 - \sum_{j=1}^d |x_j|\right)^+ = \tilde{\psi}\left(x_d, \left(1 - \sum_{j=1}^{d-1} |x_j|\right)^+\right) = \tilde{\psi}(x_d, \psi_{d-1}(\tilde{\mathbf{x}})),$$

so that:

$$\psi_d(\mathbf{x}) = \varphi(x_d - \psi_{d-1}(\tilde{\mathbf{x}})) - 2\varphi(x_d) + \varphi(x_d + \psi_{d-1}(\tilde{\mathbf{x}})). \quad (21)$$

The latter is a recursive expression for ψ_d , starting from $\psi_0 = 1$ that can be used to construct a DAC neural network computing this function.

We have already seen that ψ_1 can be obtained as a 1 layer, 1 unit DAC network with 3 (replicated) input nodes. Then $x_2 + 1 = \varphi(x_2 + 1)$ can also be obtained as 1 unit on the first layer (with one input node); by linearity, the same holds for the two terms $\varphi(x_2 + 1) \pm \psi_1(x_1)$, with 4 input nodes (x_1 replicated thrice and x_2 taken once). Then:

$$\psi_2(x_1, x_2) = \varphi(-1 + x_2 + 1 - \psi_1(x_1)) - 2\varphi(-1 + x_2 + 1) + \varphi(-1 + x_2 + 1 + \psi_1(x_1))$$

can be obtained as a 2-layer DAC network, with 1 unit (with 3 inputs and all DAC biases equal to -1) in layer 2 and 3 units (with 4, 1, and 4 input nodes) in layer 1.

One can generalize this approach to a higher dimension $d \geq 3$ as follows. Let τ_i denote $\psi_i(x_1, \dots, x_i)$, for the sake of simplicity. In the generic layer $i = 2, \dots, d-1$ there will be two DAC units (with 4 input nodes and three biases equal to -1) computing:

$$\begin{cases} x_{i+1} + 1 + \tau_i = \varphi(x_{i+1} + 1) + \varphi(-1 + x_i + 1 - \tau_{i-1}) - 2\varphi(-1 + x_i + 1) + \varphi(-1 + x_i + 1 + \tau_{i-1}) \\ x_{i+1} + 1 - \tau_i = \varphi(x_{i+1} + 1) - \varphi(-1 + x_i + 1 - \tau_{i-1}) + 2\varphi(-1 + x_i + 1) - \varphi(-1 + x_i + 1 + \tau_{i-1}) \end{cases} \quad (22)$$

and $d - i$ additional units to pass on the variables x_{i+1}, \dots, x_d , through $x_j + 1 = \varphi(x_j + 1)$. Layer 1 will be similar but with $\tau_0 = 1$. Layer d will have just 1 unit, computing:

$$\psi_d(\mathbf{x}) = \tau_d = \varphi(-1 + x_d + 1 - \tau_{d-1}) - 2\varphi(-1 + x_d + 1) + \varphi(-1 + x_d + 1 + \tau_{d-1}).$$

It's straightforward to see that this DAC network computes $\psi_d(\mathbf{x})$ following the recursion given by (21), using d layers with $d + 1, d, \dots, 4, 3, 1$ units in this order (see also Figure 6).

Later we will need to merge shifted copies $\psi_d(\mathbf{x} - \mathbf{c})$ of this function, for several values of \mathbf{c} , and this can be done efficiently by sharing the $d - i$ additional units of layer i and duplicating just the two units of equation (22). Let $\tau_i := \psi_i(x_1 - c_1, \dots, x_i - c_i)$ and $\tau_0 = 1$. Then at layer i , we can have a DAC unit with inputs and biases

input	bias
$x_{i+1} + 1$	0
$x_i + 1 - \tau_{i-1}$	$-1 - c_i$
$x_i + 1$	$-1 - c_i$
$x_i + 1 + \tau_{i-1}$	$-1 - c_i$

computing:

$$x_{i+1} + 1 + \tau_i = \varphi(x_{i+1} + 1) + \varphi(-1 - c_i + x_i + 1 - \tau_{i-1}) - 2\varphi(-1 - c_i + x_i + 1) + \varphi(-1 - c_i + x_i + 1 + \tau_{i-1})$$

and analogously a second DAC unit will compute $x_{i+1} + 1 - \tau_i$. In particular, these two units compute functions of \mathbf{x} that depend also on \mathbf{c} and hence must be duplicated for different \mathbf{c} , but the units transporting $x_j + 1$ for $j = i + 1, \dots, d$ should be shared.

The second step is rescaling ψ_d with a positive constant $\delta > 0$ and the normalization coefficient $C_d = 2^{-d}(d + 1)!$ that makes the integral equal to 1, yielding an approximation of the Dirac delta $\psi_{d,\delta} : \mathbb{R}^d \rightarrow \mathbb{R}$:

$$\psi_{d,\delta}(\mathbf{x}) := C_d \delta^{-d} \psi_d(\delta^{-1} \mathbf{x}). \quad (23)$$

To ensure that also $\psi_{d,\delta}$ can be realized as a DAC network of the same structure as ψ_d , we observe that for a DAC unit g defined by $g(\mathbf{x}) = \sum_{j=1}^n w_j \varphi(b_j + x_j)$ and for $\lambda > 0$:

$$g(\lambda \mathbf{x}) = \sum_{j=1}^n w_j \varphi(b_j + \lambda x_j) = \sum_{j=1}^n \lambda w_j \varphi(b_j/\lambda + x_j) =: \tilde{g}(\mathbf{x})$$

so that given any multi-layer DAC network h , by simply changing the coefficients of the units in the first layer, it is possible to obtain another DAC network \tilde{h} such that $\tilde{h}(\mathbf{x}) = h(\lambda \mathbf{x})$. By linearity, the outer coefficient $C_d \delta^{-d}$ can be absorbed into the weights of the last layer, and we get $\psi_{d,\delta} \in \mathcal{G}_d$ with the same structure of ψ_d .

The third and last step of the proof is similar to the case $d = 1$. First, we consider the convolution operator $T_{d,\delta}(f) := f * \psi_{d,\delta}$, which by the approximation property of the convolution ensures that:

$$\forall f \in C^0([-1, 1]^d), \forall \varepsilon > 0, \exists \delta > 0 \text{ s.t. } \|f - f * \psi_{d,\delta}\|_\infty < \varepsilon/2. \quad (24)$$

Then, fixed f , we approximate the integral in (24) with a finite sum. To this aim, let $h(\mathbf{y}, \mathbf{x}) := f(\mathbf{y})\psi_{d,\delta}(\mathbf{x} - \mathbf{y})$, so that $f * \psi_{d,\delta}(\mathbf{x}) = \int h(\mathbf{y}, \mathbf{x}) d\mathbf{y}$. Choose a partition of $[-1, 1]^d$ by a large number k of small sets (e.g. cubes) of average volume $2^d/k$. Consider a set \mathcal{C} of k points, one for each of the sets (e.g. the center points of the cubes). Since h is continuous and the hyper-cube is compact, there exists a partition fine enough that for all \mathbf{x} :

$$\left| \int_{[-1, 1]^d} h(\mathbf{y}, \mathbf{x}) d\mathbf{y} - \sum_{\mathbf{c} \in \mathcal{C}} h(\mathbf{c}, \mathbf{x}) \frac{2^d}{k} \right| < \varepsilon/2.$$

Therefore we define $g(\mathbf{x}) := \sum_{\mathbf{c} \in \mathcal{C}} 2^d k^{-1} h(\mathbf{c}, \mathbf{x})$, yielding $\|f * \psi_{d,\delta} - g\|_\infty < \varepsilon/2$ and so $\|f - g\|_\infty < \varepsilon$.

Finally, g can be realized as a DAC neural network with d layers, since the same holds for $\psi_{\delta,d}$, and we need only to compute a linear combination of the output of k translated versions of the latter:

$$g(\mathbf{x}) := \sum_{\mathbf{c} \in \mathcal{C}} 2^d k^{-1} f(\mathbf{c}) \psi_{d,\delta}(\mathbf{x} - \mathbf{c}) =: \sum_{\mathbf{c} \in \mathcal{C}} w_{\mathbf{c}} \psi_{d,\delta}(\mathbf{x} - \mathbf{c}).$$

By linearity, $g \in \mathcal{G}_d$, can be realized as a DAC network with d layers and recalling that only two units in each layer must be duplicated to account for different values of \mathbf{c} , while the others can be shared, we get that the layers $1, 2, \dots, d$ have respectively $2k + d - 1, 2k + d - 2, \dots, 2k + 2, 2k + 1, 1$ units. \square

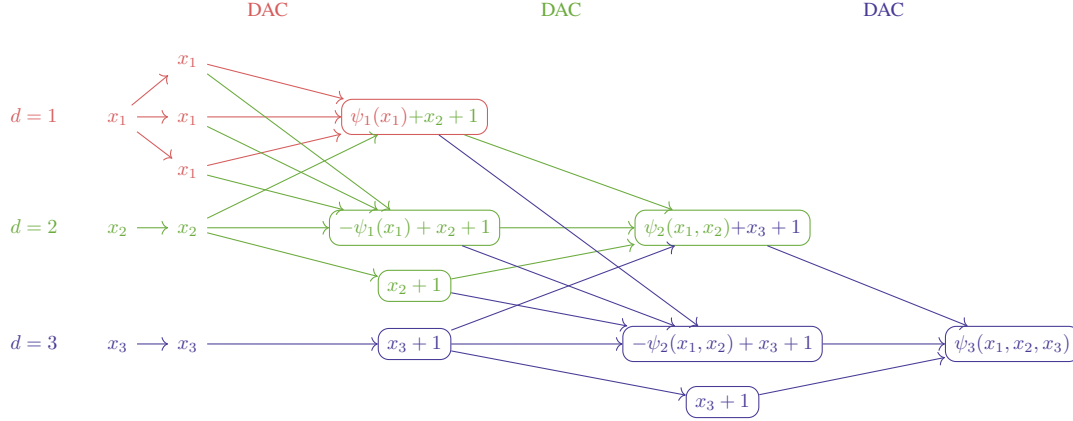


Figure 6. This figure illustrates how the d -layers network corresponding to ψ_d can be inductively built from the $d - 1$ -layers network corresponding to ψ_{d-1} , for $d = 1, 2, 3$. When $d = 1$, only the red elements in the figure exist, corresponding to (16): after replication of x_1 , the three red arrows perform preactivation with biases $-1, 1, 0$ and weights $1, 1, -2$, to produce ψ_1 . When $d = 2$, the green elements are included on top of the red ones. The new variable x_2 is taken forward as $\varphi(x_2 + 1) = x_2 + 1$ and combined with the appropriate weights to produce 3 ReLU arguments needed in (21) for $d = 2$. These are the new layer 1 outputs, that are combined with weights $1, 1, -2$ (and DAC biases $-1, -1, -1$ to recover the original value of x_2), to produce the layer 2 output ψ_2 . When $d = 3$, the blue elements are included on top of the red and green ones. The same operations performed for $d = 2$ with the red network nodes are now performed with the green network nodes, but 1 layer forward. This produces the layer 3 output ψ_3 .

Remark D.2. Case $d = 1$ in Theorem D.1 shows that a single-layer DAC neural network is a universal approximator in $C^0([-1, 1])$. This is not true for a standard single-layer neural network, where input replication has no effect.

Remark D.3. Proof of Theorem D.1 can be easily extended to functions with compact support.

Remark D.4. We observe that the d -dimensional spike function ψ_d appearing in the proof, can also be realized as a 2-layer DAC network as follows:

$$\psi_d(\mathbf{x}) = \varphi\left(1 - d + \sum_{j=1}^d [\varphi(x_j + 1) - 2\varphi(x_j)]\right).$$

In fact, $\varphi(x + 1) - 2\varphi(x)$ is positive only for $|x| < 1$, and equals $1 - |x|$ on that interval. Therefore, the sum above is equal to $d - \|\mathbf{x}\|_1$ inside $[-1, 1]^d$ and lesser than $d - 1$ outside, so thanks to the outer φ , we obtain ψ_d everywhere.

Using this construction, one could prove a result similar to Theorem D.1, but with a DAC network with 2 layers, regardless of d . This network won't be sparse, as here we are trading a d -layers-deep representation with 4 or fewer input nodes per unit, for a shallow one with $2d$ input nodes per unit.